

MIT Open Access Articles

Thermal Conductivity and Flash Temperature

The MIT Faculty has made this article openly available. **Please share** how this access benefits you. Your story matters.

Citation: Reddyhoff, Tom et al. "Thermal Conductivity and Flash Temperature." Tribology Letters 67 (March 2019): 22 © The Author(s)

As Published: <https://doi.org/10.1007/s11249-018-1133-8>

Publisher: Springer-Verlag

Persistent URL: <https://hdl.handle.net/1721.1/121231>

Version: Final published version: final published article, as it appeared in a journal, conference proceedings, or other formally published context

Terms of use: Creative Commons Attribution 4.0 International license





Thermal Conductivity and Flash Temperature

Tom Reddyhoff¹ · Aaron Schmidt² · Hugh Spikes¹

Received: 19 October 2018 / Accepted: 29 December 2018
© The Author(s) 2019

Abstract

The thermal conductivity is a key property in determining the friction-induced temperature rise on the surface of sliding components. In this study, a Frequency Domain Thermoreflectance (FDTR) method is used to measure the thermal conductivity of a range of tribological materials (AISI 52100 bearing steel, silicon nitride, sapphire, tungsten carbide and zirconia). The FDTR technique is validated by comparing measurements of pure germanium and silicon with well-known values, showing discrepancies of less than 3%. For most of the tribological materials studied, the thermal conductivity values measured are reasonably consistent with values found in the literature. However the measured thermal conductivity of AISI 52100 steel (21 W/mK) is less than half the value cited in the literature (46 W/mK). Further bulk thermal conductivity measurements show that this discrepancy arises from a reduction in thermal conductivity of AISI 52100 due to through-hardening. The thermal conductivity value generally cited and used in the literature represents that of soft, annealed alloy, but through-hardened AISI 52100, which is generally employed in rolling bearings and for lubricant testing, appears to have a much lower thermal conductivity. This difference has a large effect on estimates of flash temperature and example calculations show that it increases the resulting surface temperatures by 30 to 50%. The revised value of thermal conductivity of bearing steel also has implications concerning heat transfer in transmissions.

Keywords Flash temperature · Thermal conductivity measurement · 52100 steel · Scuffing · Lubrication

1 Introduction

In a sliding or rolling-sliding contact the heat dissipation rate is given by;

$$\dot{Q} = \mu W u_s \quad (1)$$

where μ is the friction coefficient, W the applied load and u_s the velocity difference between the two surfaces, i.e. the sliding speed. For high pressure, non-conforming contacts such as are present in gears and sliding cam-follower components, where the load is applied over a very small contact area and sliding speeds can be considerable, this can produce large and very rapid rises in temperature of the two surfaces

known as flash temperatures [1, 2]. Here the intensity of heat generation coupled with the finite thermal diffusivity of one or both the contacting bodies produces a local and transient temperature rise just a few microns deep into the surface as the latter traverses the contact. This flash temperature rise is believed to influence several important tribological processes including scuffing [3–5], elastohydrodynamic friction [6, 7] and some types of tribofilm formation [8, 9].

The precise calculation of flash temperature rise is complex and involves moving heat source theory. However, because of its practical importance in tribology, approximate calculation methods have been developed that are able to estimate the magnitude of flash temperature based on a knowledge of the heat dissipation rate, the size and geometry of the contact, the velocities with which the two surfaces traverse the contact and the thermal diffusivities and conductivities of the surfaces [10–14]. The thermal diffusivity of a material is defined by $\chi = K / \rho \sigma$ where K is its thermal conductivity, ρ its density and σ its specific heat. For surfaces that move across the contact at high speed the flash temperatures rise increases with the inverse of the square

Electronic supplementary material The online version of this article (<https://doi.org/10.1007/s11249-018-1133-8>) contains supplementary material, which is available to authorized users.

✉ Hugh Spikes
h.spikes@imperial.ac.uk

¹ Imperial College London, London, UK

² Massachusetts Institute of Technology, Cambridge, MA, USA

root of the thermal diffusivity, while in low speed sliding it varies inversely with the thermal conductivity.

In practical terms this means that in order to calculate flash temperatures it is necessary to know the thermal properties of the contacting materials. For density and specific heat this is reasonably straightforward, at least if it is assumed that the near-surface properties are the same as the bulk properties. The latter can be quite easily measured or reliable values found in the literature. However thermal conductivity is more problematic since often only generic values are available in the literature and thermal conductivity is much less easily measured. Reliable thermal conductivities are available for pure elements but not necessarily for alloys such as steels or for composites. With alloys it is also questionable whether the near-surface composition is sufficiently similar to the bulk composition for bulk thermal conductivity to be useful.

To address this issue the current paper describes measurement of the thermal conductivities of various materials relevant to tribology, using a technique designed to interrogate the conductivity of the near-surface and thus be directly applicable to flash temperature calculation.

2 Test Method

Thermal conductivities were measured using Frequency Domain Thermoreflectance (FDTR) [15, 16]. Two continuous wave diode lasers are directed at the material of interest, one acting as a heat source (the pump) and the other detecting resulting changes in temperature from changes in surface reflectivity (the probe). The microscope set-up is shown schematically in Fig. 1 [16]. The pump is a 50 mW diode laser with a wavelength of 785 nm, digitally modulated by the reference output of a lock-in amplifier, and the probe is a 20 mW diode laser with a wavelength of 532 nm. The lock-in detects the phase lag in the probe signal relative to the reference output signal. A balanced photodetection scheme is used to improve signal to noise ratio. A flip mirror is employed to temporarily direct a portion of the pump beam to the signal photodiode PD1 and determine the absolute phase of the pump beam at the sample surface. The modulation frequency of the pump beam is varied and by fitting the phase of the thermal wave at the sample surface in different frequency ranges, FDTR can extract combinations of geometrical and thermal properties [15, 16]. For example, in bulk samples it can be used to measure the heat capacity and the thermal conductivity, both the in-plane and cross-plane thermal conductivities of anisotropic samples or the thickness and thermal conductivity of buried layers. In this study, imaging FDTR was employed to enable micron-scale resolution maps of thermal conductivity. For this, the

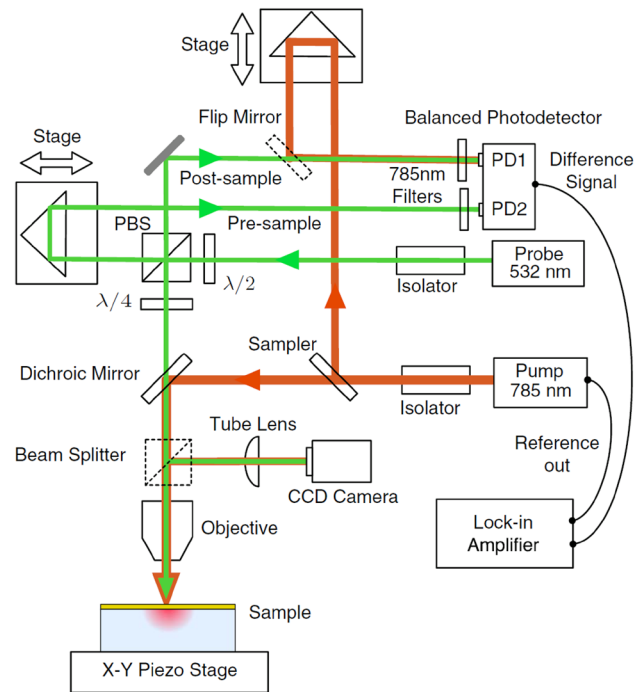


Fig. 1 FDTR microscope based on two lasers. Figure reproduced from ref. [16]

specimen was mounted on an x – y piezo stage and the sample was coated with a thin (~ 100 nm) gold layer with a high coefficient of thermoreflectance at the probe wavelength to maximise signal strength.

The uncertainty of the data-fitting process has been explored using a Monte Carlo simulation of the data-fitting process, assuming typical uncertainty in the known model parameters (gold coating thickness, heat capacity and thermal conductivity). Results for the volumetric heat capacity and thermal conductivity of the silicon are shown in Fig. 2 and indicate precision of $ca \pm 4\%$ for this sample.

In the current study all measurements were made at room temperature (293 ± 2 K) and for each sample thermal conductivity imaging was used to check for sample uniformity and to find suitable locations for measurement. At least five measurements were made on each sample.

3 Test Materials

Two test materials relevant to tribology were of particular interest in this study; AISI 52100 steel and tungsten carbide. AISI 52100 (aka SUJ2, 100Cr6, 535A99) is a very widely-used bearing steel and is also often employed as test specimens in friction, wear and scuffing tests on equipment such as the four ball tester and the mini-traction machine (MTM). Tungsten carbide is used in cutting tools and mechanical seals and also in EHD traction testing

in disc machines and in the MTM, since its high elastic modulus enables high contact pressures to be reached at relatively low applied loads. In this study both MTM balls (diameter 19.5 mm) and MTM discs were used in these materials. Also studied were zirconia balls that are used in ball milling applications as well as in rolling bearings in corrosive media, and silicon nitride ball bearings, which are widely employed in very high speed rolling bearings. Zirconia has an unusually low thermal conductivity and so is also used as a thermal barrier coating. Another material of interest was sapphire. This is transparent to thermal infrared wavelengths and is thus often employed as one surface in research studies that use infrared emission to measure temperature rise in contacts [17, 18].

Tests were also carried out on two other, well-defined test materials of known thermal conductivity in order to validate the thermal conductivity method. These were undoped silicon (Si) and undoped germanium (Ge). The Si and Ge samples were treated with an HF solution to remove native oxide. All samples were e-beam coated with 120 nm of gold.

The material samples studied are listed in Table 1 together with their nominal thermal conductivities taken from the literature references shown. Values cited are at *ca* 293 K and it should be noted that thermal conductivity decreases with increasing temperature. The thermal conductivities of WC, ZnO₂ and Si₃N₄ are problematic since for engineering applications components are generally produced from sintered powder so that the conductivity can depend on original particle size and also in some cases the presence and concentration of binding or stabilising materials. The hardness of the AISI 52100 MTM ball was 855 ± 15 HV and that of the disc 815 ± 15 HV.

4 Results

Results of the form shown in Figs. 2 and 3 were obtained for all samples and are included in Supplementary Information. The resulting calculated thermal conductivities and specific heats are listed in Table 2, along with the ± 1/e confidence interval accounting for both experimental noise and the uncertainty in the model parameters. It should be noted that the specific heats are volumetric rather than having the more normally units kJ/kgK.

Comparison of Tables 1 and 2 show that the thermal conductivity values for silicon, germanium and sapphire measured in this study are in close agreement with other values in the literature, while the value for ZrO₂ is also quite similar (and very low). Measured values for WC and Si₃N₄ are somewhat lower than most values cited in the literature, while the value for AISI 52100 steel is less than half that generally suggested and applied in tribological calculations.

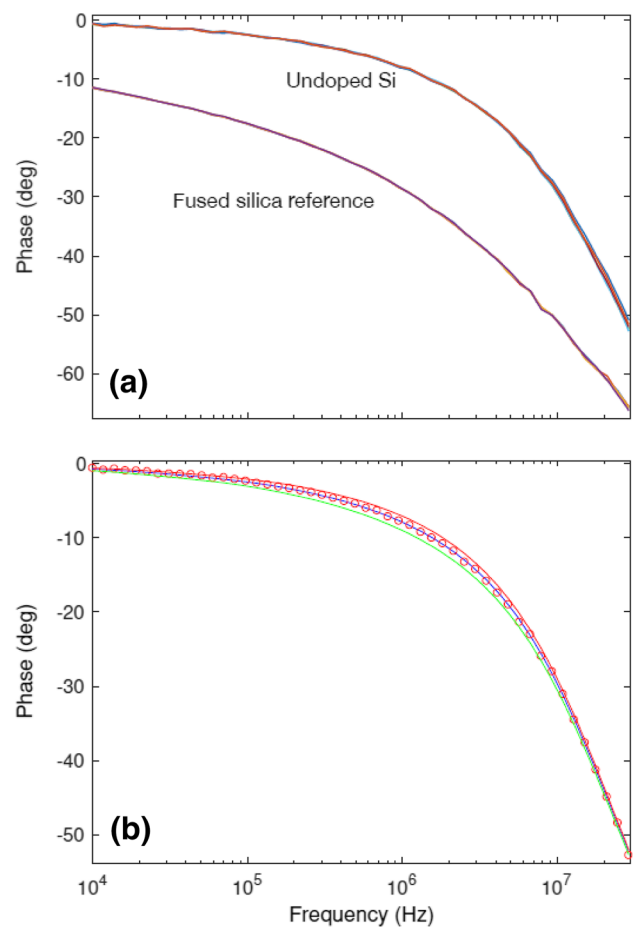


Fig. 2 **a** Phase vs. modulation frequency data from five locations on the undoped silicon samples, along with data from the fused silica reference sample. **b** Sample data (red circles) and best model fit (blue line) for one of the locations on the Si sample. Red and green lines show the model solutions obtained by varying the thermal conductivity by ±20%

Possible reasons for these differences and their implications are discussed below.

5 Discussion

5.1 Thermal Conductivity Measurements

The depth of the FDTR measurements depends on the material and the property being measured, but is typically < 10 μm. The depth the thermal waves penetrate into the material is given by the formula

$$d = \sqrt{\frac{2\chi}{\omega}}$$

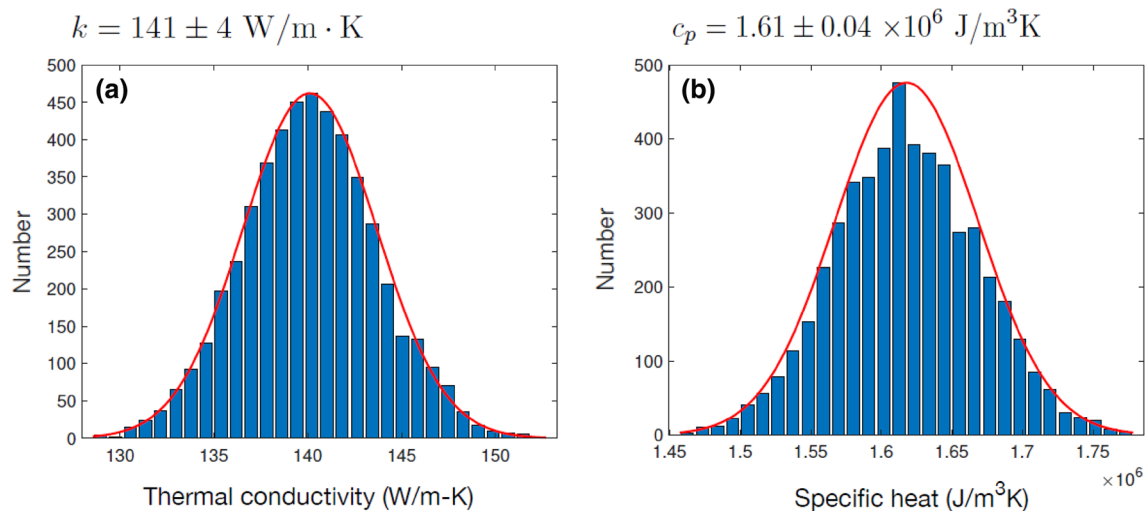


Fig. 3 Monte Carlo results of the data-fitting process for silicon from 1000 iterations, **a** Thermal conductivity, **b** Specific Heat

Table 1 Materials tested

Test material	Form	Nominal thermal conductivity (W/mK)	Ref.
AISI 52100 (steel)	MTM ball	46.6, 46	[19, 20]
AISI 52100 (steel)	MTM disc	46.6	[19]
Tungsten carbide (WC)	MTM ball	110, 80–100, 40, 84	[21–24]
Tungsten carbide (WC)	MTM disc	110, 80–100, 40, 84	[21–24]
Zirconia (ZrO ₂)	MTM ball	2.0, 1.9 (stabilised)	[25, 26]
Silicon nitride (Si ₃ N ₄)	MTM ball	30 (1% MgO)	[23]
Single crystal sapphire	MTM disc	23, 24, 42	[27, 28]
Silicon (Si)	undoped wafer	145	[29]
Germanium (Ge)	undoped wafer	55	[29]

Table 2 Materials tested; FDTR measurements

Test material		Thermal conductivity (W/mK)	Specific heat × 10 ³ kJ/m ³ K
AISI 52100 (steel)	Ball	21 ± 1	3.44 ± 0.17
AISI 52100 (steel)	Disc	21 ± 1	4.14 ± 0.20
Tungsten carbide (WC)	Ball	58 ± 2	1.46 ± 0.44
Tungsten carbide (WC)	Disc	65 ± 5	2.50 ± 0.34
Zirconia (ZrO ₂)	Ball	2.4 ± 0.5	2.40 ± 0.14
Silicon nitride (Si ₃ N ₄)	Ball	18.2 ± 0.7	1.63 ± 0.08
Single crystal sapphire		K _⊥ 30.8 ± 2.5 K _∥ 35.0 ± 2.5	
Silicon (Si)	Undoped wafer	141 ± 4	1.61 ± 0.04
Germanium (Ge)	Undoped wafer	55 ± 2	1.75 ± 0.05

where χ is the thermal diffusivity and ω is the modulation angular frequency. Figure 4 shows the penetration depth as a function of frequency for silicon and fused silica. The value obtained for silicon, for example, is for the first 10 μm from the surface, while for fused silica it is closer to 1 μm . Also, although the FDTR measurement uses a wide range of modulation frequencies, there is only sensitivity to a given physical property in a narrower range of frequencies. Thermal conductivity, for example, is most sensitive in the frequency range of roughly 1–10 MHz, while heat capacity tends to be more sensitive at lower frequencies, so the heat capacity values represent a slightly deeper layer of the sample than the thermal conductivity values. Therefore, a precise number for the depth of the measurement would be slightly different for each material and each property, but all

will be within roughly the first 10 microns from the surface. This is similar to the depth subjected to flash temperature rise for fast moving heat sources.

Figures 5 and 6 below show maps of measured thermal conductivities of the tungsten carbide ball and disc and the zirconia ball. The map for zirconia shows quite constant conductivity over the surface studied, but that of tungsten carbide shows considerable variations of thermal conductivity across the surface. This may reflect either pores having very low thermal conductivity (as seen WC ball map), or the distribution of a second component. For some specimens it is likely that these variations reflect the roughness of the specimen surfaces. In fact, the roughness of the Si₃N₄ specimen was too high to enable reflectance measurements to be made over the whole surface. For this reason, for the

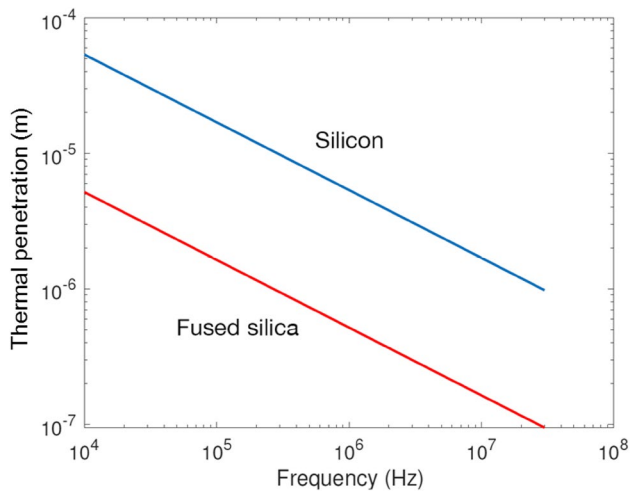


Fig. 4 Penetration depth as a function of frequency for silicon and fused silica

Si_3N_4 sample, the thermal conductivity measurements for Table 2 were made only on the regions of the surface showing sufficient reflectance. The location of these measurement regions are indicated in the intermediate phase maps in Supplementary Information.

5.2 Thermal Conductivity of AISI 52100 Steel

The most striking finding of this study is that both the AISI 52100 steel MTM balls and discs tested exhibit thermal conductivity less than half the values generally cited in the literature. Thermal conductivity maps for these specimens are shown in Fig. 7. They do not show the level of heterogeneity seen with WC, though there is some spatial variation. Clearly the origins of this discrepancy between the literature values and those found in this study are of interest. It is

noteworthy that both the MTM ball and disc show similar thermal conductivities although they originated from quite different manufacturers and, presumably steel sources. This suggests that the low thermal conductivity found in the current study is general and not just a result of a batch of out-of-specification material.

The discrepancy between the literature values and those measured in this study might have one of two broad origins. One is it represents a difference in near-surface structure or composition arising from the manufacturing process between AISI 52100 samples used in the past to determine thermal conductivity and the current MTM specimens. This might result from, for example grain refinement or increased carbide composition of the alloy close to the surface. Most traditional methods of determining thermal conductivity measure a bulk property but FDTR values are obtained within about 10 μm of the surface. It should be noted that if this were the case, FDTR are likely to be more applicable to flash temperature calculations. Alternatively it might represent a difference in the bulk thermal conductivity between the material used to obtain the literature values and that of the specimens tested in the current study.

Both possibilities were examined by obtaining new measurements of the bulk thermal conductivity of AISI 52100 steel from the National Physical Laboratory (NPL, Teddington UK) using a laser flash apparatus. In this, a short laser pulse is applied to one flat face of a disc specimen and the transient temperature rise of the opposite face is monitored with an infrared detector. From this the thermal diffusivity can be measured and this, combined with parallel specific heat and density measurements, enables calculation of thermal conductivity. To avoid having to machine specimens to fit the apparatus, high frequency reciprocating rig (HFRR) AISI 52100 disc specimens having diameter 10 mm and thickness 3 mm were studied. HFRR discs of two hardness

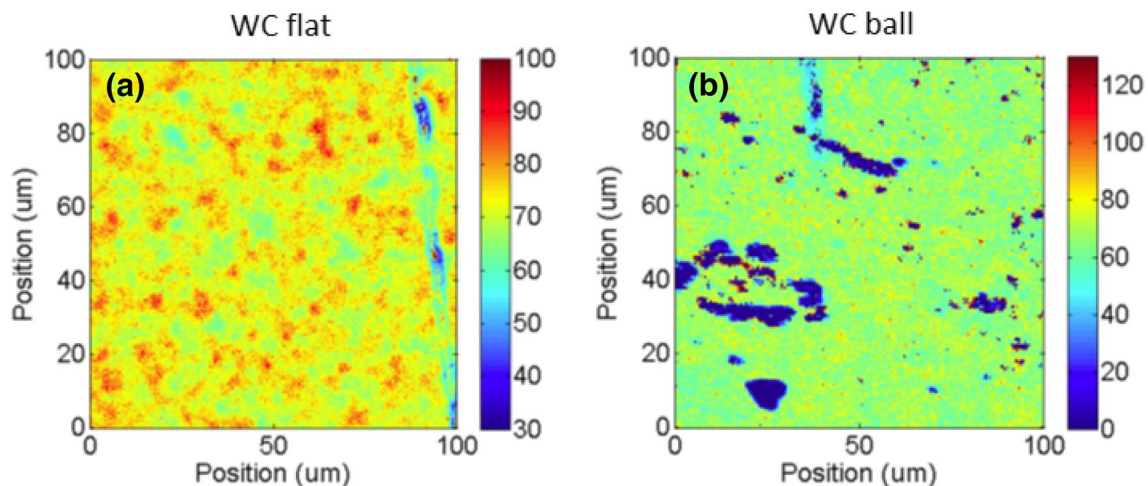


Fig. 5 Thermal conductivity maps for the measured specimens, **a** WC disc, **b** WC ball; (colour scale units are W/mK)

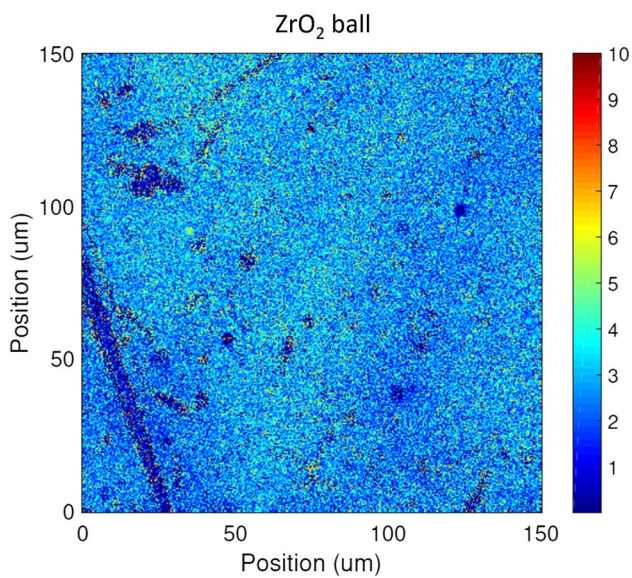


Fig. 6 Thermal conductivity maps for the zirconia ball: (colour scale units are W/mK)

were tested; standard ones used in fuel lubricity testing [30] with hardness 196 HV and through-hardened ones often used in lubricant studies, having hardness 772 HV.

The measured bulk thermal properties of the two discs are listed in Table 3. The thermal conductivities of the two HFRR discs are quite different from one another. The soft disc has thermal conductivity comparable to the values found in the literature and the hard one has conductivity similar to the FDTR measured value for MTM specimens. The specific heats measured are quite close to the MTM specimen values obtained using FDTR,

It thus appears likely that the current literature values of the thermal conductivity of AISI 52100 are based on measurements (or perhaps just one historic measurement) of the annealed alloy, and that through-hardening to produce steel for useful bearing components results in a large decrease in conductivity. This may originate from differences between the largely pearlitic annealed structure and the largely martensitic quenched and tempered one.

5.3 Flash Temperature Implications

It is of interest to assess the impact of hard AISI 52100 specimens having a thermal conductivity value of 21 W/mK rather than the 46 W/mK normally used to estimate flash temperature rise.

As an example, a 19.5 mm diameter steel ball sliding against steel flat contact under a load of 30 N is considered. Two types of motion are analysed; (i) a stationary ball sliding against the flat (pure sliding), as typically present in a pin-on-disc configuration and (ii) both surfaces moving with an entrainment (mean) speed of 3 m/s but with the flat moving faster than the ball, as often used in EHD traction studies. The slide-roll ratio is then the ratio of the sliding speed to the entrainment speed. The flash temperature calculation method is described

Table 3 Bulk thermal property measurements from NPL

Disc hardness	Thermal conductivity (W/mK)	Density (kg/m ³)	Specific heat (kJ/kgK)	Specific heat $\times 10^3$ kJ/m ³ K
196 VPN	41 \pm 1	7723	0.446	3.445
772 VPN	26.1 \pm 0.2	7704	0.446	3.436

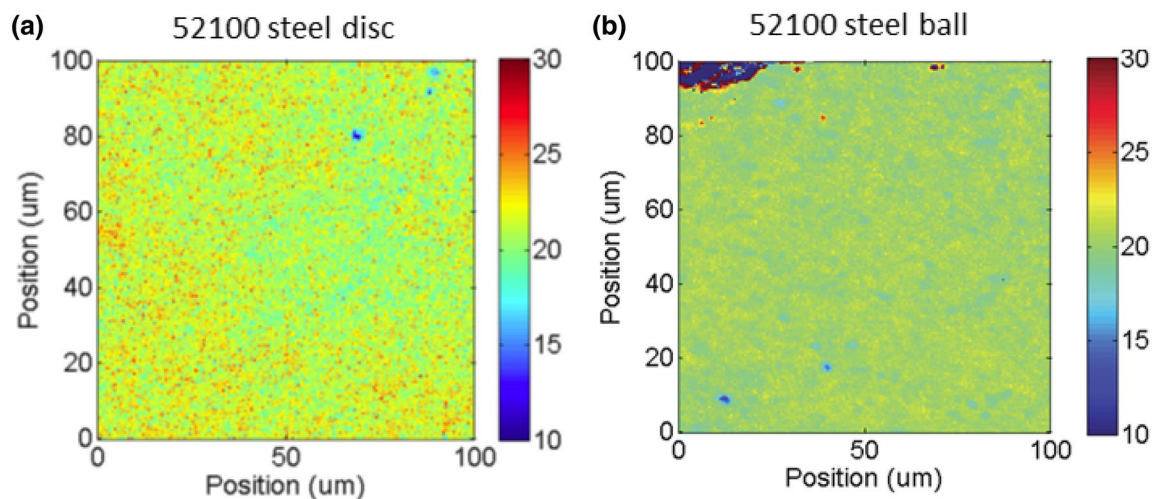


Fig. 7 Thermal conductivity maps for the steel disc and ball specimens, **a** steel disc, **b** steel ball; (colour scale units are W/mK)

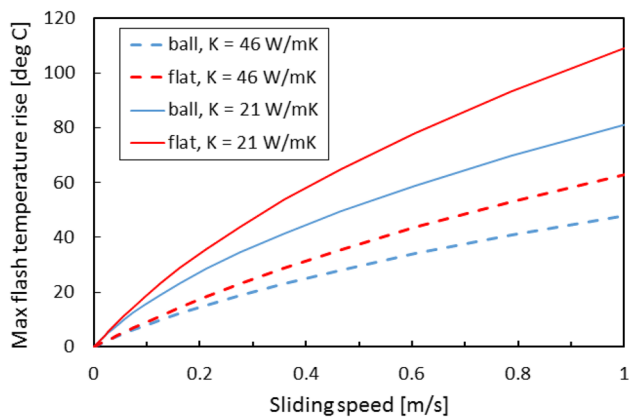


Fig. 8 Calculated maximum flash temperature rise as a function of sliding speed for sliding pin-on-disc contact, 30N load

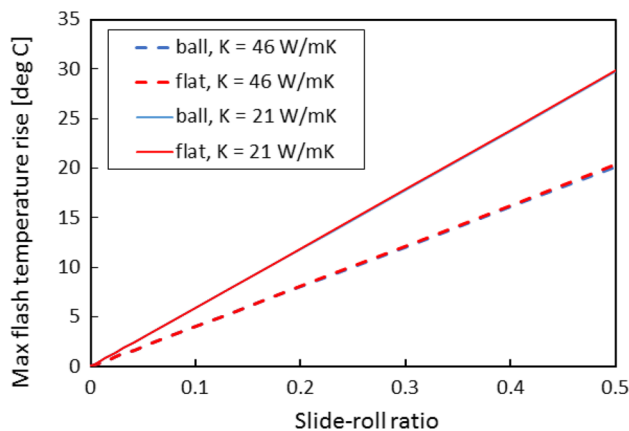


Fig. 9 Calculated maximum flash temperature as a function of slide-roll-ratio for rolling/sliding ball-on-disc contact at 30N load and 3 m/s entrainment speed (ball and flat show almost identical flash temperatures)

in the [Appendix](#). Figure 8 compares the maximum flash temperature rise of the stationary ball and the moving flat over a range of sliding speeds, taking the thermal conductivity to be both the measured value of 21 W/mK and a commonly used value of 46 W/mK. The friction coefficient is assumed to be 0.1, the density of steel 7710 kg/m³ and the specific heat 440 J/kgK. The Hertzian contact radius is 129 μm . It can be seen that the calculated flash temperature rise based on $K = 21$ W/mK is twice as high at low speeds and two-thirds higher at high sliding speed than that calculated from the conventional value.

Figure 9 shows predictions for the rolling-sliding system. The contact conditions are the same as the pure sliding example except that the friction coefficient is taken to

be 0.05, typical of EHD values. The ball and flat temperature rises are very similar and effectively superimposed. Again the lower value of thermal conductivity of 21 W/mK produces considerably higher flash temperature rise, about 50% higher than that obtained using $K = 46$ W/mK over the whole range of rolling-sliding conditions.

6 Conclusions

A Frequency Domain Thermoreflectance (FDTR) method has been used to measure the thermal conductivity of a range of materials of tribological interest as well as two reference materials. This method has four advantages over more conventional methods of measuring the thermal conductivity of solids for application to tribology.

- i. It measures the near-surface thermal conductivity rather than that of the bulk material. The former has greater relevance than the latter to flash temperature rise during sliding since flash temperature rises occur within the near-surface
- ii. It measures the thermal conductivity of the surfaces of bodies with complex shapes as present in finished engineering components, including ball bearings, without requiring special samples to be cut from the material of interest
- iii. It is able to map the thermal conductivity across a surface and thus provide insights into how this varies spatially for composite materials
- iv. Although not tested in the current study FDTR can also measure the thermal conductivity of coated and surface-treated components such as case-carburised ones, which is not possible using bulk measurement methods.

For the reference materials studied (silicon and germanium) the measured thermal conductivity values are very close to literature values. The values measured for tungsten carbide lie within the wide range of literature values available and reflect the composite nature of the powder forged material used in most engineering applications.

Both samples of AISI 52100 steel tested show thermal conductivity of 21 W/mK, which is less than half the value normally provided in the literature. This difference means that flash temperature rises are currently being under-predicted in sliding and rolling-sliding contacts by about 50%. From bulk thermal conductivity measurements on AISI 52100 specimens of different hardness it appears that the value of 46 W/mK generally cited in the literature is based on measurement of annealed 52100 steel specimens and that through-hardening to produce useful bearing components results in a large drop in thermal conductivity. As

well as being important in the context of tribological contacts, this finding also has important implications on heat flow in transmissions, with consequent effects on overall performance.

Acknowledgements The authors are grateful to Petra Mildeova of the National Physical Laboratory for conducting the laser flash apparatus measurement of thermal conductivity.

Open Access This article is distributed under the terms of the Creative Commons Attribution 4.0 International License (<http://creativecommons.org/licenses/by/4.0/>), which permits unrestricted use, distribution, and reproduction in any medium, provided you give appropriate credit to the original author(s) and the source, provide a link to the Creative Commons license, and indicate if changes were made.

Appendix

In flash temperature calculations, two asymptotic solutions are generally used, one when the surface moves very slowly across the heat source contact and one when it traverses the heat source rapidly. These represent respectively the two relatively simple solutions, one in which the heat source is stationary and one in which lateral conduction is neglected. The non-dimensional speed of the surface relative to the contact is defined by $J = ub/\chi$ where u is the speed of the surface relative to the contact (and thus the heat source), b is the half width or half diameter of the contact and χ the thermal diffusivity. Francis [12] and Greenwood [14] have provided equations for maximum flash temperature rise of surfaces passing across a circular Hertzian contact, as present in a ball loaded and sliding against a flat;

$$\theta_{\text{slow,max}} = \frac{3}{8} \frac{\dot{Q}_{\text{in}}}{bK} \quad (2)$$

$$\theta_{\text{fast,max}} = 0.5895 \frac{\dot{Q}_{\text{in}}}{bKJ^{0.5}} \quad (3)$$

where \dot{Q}_{in} is the rate at which heat enters the surface, K the thermal conductivity and $\theta_{\text{slow,max}}$ and $\theta_{\text{fast,max}}$ are the slow and fast asymptotic solutions.

Greenwood [14] has developed a simple interpolation method for calculating flash temperature rise at intermediate temperatures based on;

$$\frac{1}{\theta_{\text{max}}^2} = \frac{1}{\theta_{\text{slow,max}}^2} + \frac{1}{\theta_{\text{fast,max}}^2} \quad (4)$$

and from this interpolation, an expression for the maximum flash temperature rise at any speed is obtained by combining Eqs. 2, 3 and 4;

$$\theta_{\text{max}} = \frac{\dot{Q}_{\text{in}}}{bK} \frac{0.5895}{\sqrt{J + 2.471}} \quad (5)$$

The total rate of heat generation, \dot{Q} , is easily calculated from Eq. 1, but this heat is partitioned between the two surfaces with $\alpha\dot{Q}$ entering one surface and $(1 - \alpha)\dot{Q}$ the other. More heat generally enters the faster moving surface since its motion helps carry heat away from the contact. Solution of Eq. 5 for the two surfaces thus requires evaluation of the heat partition fraction α . This value is generally calculated by assuming that the mean temperature of the two contacting surfaces is the same, and then the resulting heat partition fraction is used to evaluate the maximum temperatures of the two surfaces.

Francis gives mean flash temperature rise asymptotes for the Hertzian contact case as [12];

$$\theta_{\text{slow,mean}} = \frac{9}{32} \frac{\dot{Q}_{\text{in}}}{bK} \quad (6)$$

$$\theta_{\text{fast,mean}} = 0.3654 \frac{\dot{Q}_{\text{in}}}{bKJ^{0.5}} \quad (7)$$

so the mean rise at any intermediate temperature from Eq. 4 is;

$$\theta_{\text{mean}} = \frac{\dot{Q}_{\text{in}}}{bK} \frac{0.3654}{\sqrt{J + 1.299}} \quad (8)$$

It should be noted that Eq. 7 is approximate and a more accurate two term expression is also provided by Francis [12];

$$\theta_{\text{fast,mean}} = 0.3234 \frac{\dot{Q}_{\text{in}}}{bKJ^{0.5}} \left(1 + \frac{1.047}{J} + \frac{0.774}{J^{3/2}} \right) \quad (9)$$

This can be used with Eqs. 4 and 6 to derive more accurate alternative to Eq. 8, but over the conditions analysed in this paper the resulting difference in the calculated heat partition fraction is only 2%.

By equating the mean temperature rises of the two bodies, the heat partition fraction can be calculated from Eq. 10, and this can then be used to determine \dot{Q}_{in} for each surface and thus the latter's maximum flash temperature rise.

$$\alpha \frac{\dot{Q}}{bK} \frac{0.3654}{\sqrt{J_{\text{flat}} + 1.299}} = (1 - \alpha) \frac{\dot{Q}}{bK} \frac{0.3654}{\sqrt{J_{\text{ball}} + 1.299}} \quad (10)$$

$$\frac{(1 - \alpha)}{\alpha} = \frac{\sqrt{J_{\text{ball}} + 1.299}}{\sqrt{J_{\text{flat}} + 1.299}} \quad (11)$$

References

1. Blok, H.: Theoretical study of temperature rise at surfaces of actual contact under oiliness lubricating conditions. Proc. Inst. Mech. Eng. Conf. Gen. Discuss. Lubr. **2**, 222–235 (1937)
2. Blok, H.: The flash temperature concept. Wear **6**, 483–494 (1963)

3. Blok, H.: Lubrication as a gear design factor. Proc. Intern. Conf. Gearing Inst. Mech. Eng. Lond. **19**, 144–158 (1958)
4. Dyson, A., Naylor, H.: Application of the flash temperature concept to cam and tappet wear problems. Proc. Inst. Mech. Eng. **14**, 255–280 (1960)
5. Bowman, W.F., Stachowiak, G.W.: A review of scuffing models. Tribol. Lett. **2**, 113–131 (1996)
6. Crook, A.W.: The lubrication of rollers III. A theoretical discussion of friction and the temperatures in the oil film. Phil. Trans. R. Soc. Lond. A **254**, 237–258 (1961)
7. Spikes, H.A., Zhang, J.: History, origins and prediction of elastohydrodynamic friction. Tribol. Lett. **56**, 1–25 (2014)
8. Fischer, T.E.: Tribochemistry. Ann. Rev. Mater. Sci. **18**, 303–323 (1988)
9. Kalin, M.: Influence of flash temperatures on the tribological behaviour in low-speed sliding: a review. Mater. Sci. Eng. A **374**, 390–397 (2004)
10. Jaeger, J.: Moving sources of heat and the temperature of sliding contacts. Proc. R Soc N. S. W. **76**, 203–224: (1942)
11. Archard, J.F.: The temperature of rubbing surfaces. Wear **2**, 438–455 (1959)
12. Francis, H.A.: Interfacial temperature distribution within a sliding Hertzian contact. ASLE Trans. **14**, 41–54 (1970)
13. Kuhlmann-Wilsdorf, D.: Sample calculations of flash temperatures at a silver-graphite electric contact sliding on copper. Wear **107**, 71–90 (1986)
14. Greenwood, J.A.: An interpolation formula for flash temperatures. Wear **150**, 153–158 (1991)
15. Schmidt, A.J., Cheaito, R., Chiesa, M.: A frequency-domain thermoreflectance method for the characterization of thermal properties Rev. Sci. Instrum. **80**, 094901 (2009)
16. Yang, J., Carlo, M., Schmidt, A.J.: Thermal property microscopy with frequency domain thermoreflectance. Rev. Sci. Instrum. **84**, 104904 (2013)
17. Suzuki, S., Kennedy, F.E.: The detection of flash temperatures in a sliding contact by the method of tribo-induced thermoluminescence. Trans. ASME J. Tribol. **113**, 120–127 (1991)
18. Spikes, H.A., Anghel, V., Glovnea, R.: Measurement of the rheology of lubricant films within elastohydrodynamic contacts. Tribol. Lett. **17**, 589–600 (2004)
19. Ramesh, A., Melkote, S.N.: Modeling of white layer formation under thermally dominant conditions in orthogonal machining of hardened AISI 52100 steel. Int. J. Mach. Tools Manuf. **48**(3–4), 402–414 (2008)
20. http://www.nsk.com.br/upload/file/nsk_cat_e728g_10.pdf. Accessed 18 Oct 2018
21. Blau, W.C., Peter, J.: Wear of Materials, p. 1345. Elsevier, New York (2003)
22. <http://www.wesltd.com/divisions/hardmetal/html/Tungsten-carbide.html>. Accessed 18 Oct 2018
23. http://www.kayelaby.npl.co.uk/general_physics/2_3/2_3_7.html. Accessed 18 Oct 2018
24. Lee, S.M., Chow, H.M., Huang, F.Y., Yan, B.H.: Friction drilling of austenitic stainless steel by uncoated and PVD AlCrN- and TiAlN-coated tungsten carbide tools. Int. J. Mach. Tools Manuf. **49**, 81–88 (2009)
25. Haynes, W.M.: CRC Handbook of Chemistry and Physics. CRC press, Boca Raton (2014)
26. Ashby, M.F., Abulawi, J., Kong, H.S.: Temperature maps for frictional heating in dry sliding. Tribol. Trans. **34**, 577–587 (1991)
27. <https://www.valleydesign.com/sapprop.htm>. Accessed 18 Oct 2018
28. <https://global.kyocera.com/prdct/fc/list/material/sapphire/sapphire.html>. Accessed 18 Oct 2018
29. Maycock, P.D.: Thermal conductivity of silicon, germanium, III–V compounds and III–V alloys. Solid State Electron. **10**, 161–168 (1967)
30. ASTM: Standard test method for evaluating lubricity of diesel fuels by the high-frequency reciprocating rig (HFRR). ASTM D6079-18, (2018)